

# Virtual outcrop geology comes of age: The application of consumer-grade virtual reality hardware and software to digital outcrop data analysis

Thomas D. Seers<sup>a,\*</sup>, Ali Sheharyar<sup>b</sup>, Stefano Tavani<sup>c</sup>, Amerigo Corradetti<sup>a,d</sup>

<sup>a</sup> Petroleum Engineering Program, Texas A&M University at Qatar, Qatar

<sup>b</sup> Research Computing, Texas A&M University at Qatar, Qatar

<sup>c</sup> DiSTAR, Università di Napoli Federico II, Napoli, Italy

<sup>d</sup> Dipartimento di Matematica e Geoscienze, Università degli Studi di Trieste, Trieste, Italy

---

## ARTICLE INFO

### Keywords:

Digital outcrop  
Virtual reality  
Fracture analysis  
MATLAB language  
Remote sensing

## ABSTRACT

In this work, the application of consumer-grade virtual reality (VR) hardware and software to the analysis of digital outcrop data is explored. Here, we utilize a widely available VR hardware platform (HTC Vive) and VR based freeform 3D visual arts software package (Google Tilt Brush), to digitize fault traces from photo-textured digital outcrop models of exposures of the Penrith Sandstone Formation (Lacy's Caves), in northwest England. Using MATLAB routines provided herein, triangular meshes output from Tilt Brush are used as the basis for 3D fracture trace map extraction, which in turn, are used to generate fracture properties (trace length, orientation, areal fracture intensity). We compare the results of this analysis to two equivalent datasets obtained from the Lacy's Caves model using digital outcrop analysis deployed via a conventional flat panel display: namely (1) a 3D trace map extracted using optical ray tracing from manually interpreted calibrated images and (2) 3D traces fitted directly the Lacy's Caves textured mesh using manual polyline interpretation within an established digital outcrop analysis software platform (OpenPlot).

Fault statistics obtained using VR based analysis are broadly equivalent to those acquired from 3D trace maps extracted using the flat panel display deployed analyses presented herein. In this case study, it was found that VR based digital outcrop analysis provided faster data acquisition than the comparative pixel-based approach, which requires linkage and merging of traces mapped from multiple contiguous images. Manual raster analysis and optical ray tracing did however provide 3D trace maps with significantly higher areal fault intensity, with VR analysis incurring censoring of finer fault traces, due to the limited resolution of the outcrop model textured mesh. Whilst data acquisition times and resultant fault intensities proved similar between the VR and OpenPlot workflows, it was noted anecdotally, that the VR analysis holds some advantages for the operator when interpreting models exhibiting complex geometries, such as mine workings and caves systems, with the clip point implemented within the viewport of conventional digital outcrop analysis software tools obstructing the user from obtaining an optimum view of the outcrop surface.

VR based digital outcrop analysis techniques, such as those presented here, provide an immersive analytical environment to the operator. This allows users to fuse powerful 3D visualizations of photo-realistic outcrop models with geological interpretation and data collection, fulfilling the early promise of 'virtual outcrops' as an analytical medium that can emulate traditional fieldwork. It is hoped that this study and its associated code library will facilitate the evaluation of emerging VR technologies for digital outcrop applications, by provided access to VR analytical tools for non-specialists in virtual reality systems. Finally, prospects for the use of VR technology within the field of digital outcrop geology, as well as within the wider geosciences, are also discussed.

---

## 1. Introduction

The rapid development of close range 3D remote sensing techniques

(e.g. terrestrial lidar and structure from motion-multiview stereo photogrammetry), coupled with the commensurate development of geologically focused 3D point cloud and triangular mesh analysis

---

\* Corresponding author.

E-mail address: [thomas.seers@qatar.tamu.edu](mailto:thomas.seers@qatar.tamu.edu) (T.D. Seers).

techniques has revolutionized outcrop studies over the past decade. Indeed, the deployment of techniques for capturing and analyzing digital outcrop data is now relatively routine and provides field geologists with the means to quantitatively interrogate 3D sedimentary, structural and diagenetic architecture exposed in outcrop (e.g. Biber et al., 2018; Corradetti et al., 2021; Hodgetts, 2013; Hodgetts et al., 2015; Jones et al., 2009; Kirsch et al., 2019; Priddy et al., 2019; Pringle et al., 2006; Tavani et al., 2019; Tavani et al., 2020a; Tavani et al., 2020b; Thiele et al., 2017; Wakeford et al., 2019). Despite these advances, the medium through which such datasets have been interpreted and analyzed has largely remained the same over the past decade, with workers utilizing flat panel displays to visualize and interrogate digital outcrop models. A recent upsurge in the availability of consumer grade virtual reality (VR) hardware and software offers great potential to geoscience practitioners to visualize and interpret digital outcrop datasets within a fully immersive environment. Harnessing such technology may help to fulfill the promise of digital outcrop datasets in providing a ‘virtual’ experience of fieldwork identified by early workers (e.g. Pringle et al., 2006), but restricted hitherto by our reliance upon flat panel displays as a medium for visualization. And though examples of utilizing turnkey augmented/virtual reality hardware and software solutions for geoscientific applications are starting to emerge (e.g. Barnes et al., 2018; Boghosian et al., 2019; Caravaca et al., 2019; Le Mouélic et al., 2018), such studies are largely focused upon the visualization of digital outcrop datasets in the virtual environment, and have limited capacity to quantitatively interrogate and analyze digital rock surface models.

Despite their potential, a paucity of geologically focuber sed software tools represents a major obstacle in the deployment of virtual reality systems for geological applications. In this work, the need for discipline-specific analysis tools is approached by harnessing a consumer grade virtual reality system (HTC Vive) and freeform 3D visual arts software package (Google Tilt Brush) to interactively interpret and analyze sedimentary and structural architecture (bedding contacts, faults, fractures) from digital outcrop models. Having generated these interpretations, users utilize a script library developed in the MATLAB™ language to extract geologically useful data (e.g. orientation, length, intensity) from interactively generated 3D mesh patches output by Tilt Brush. It is hoped that by repurposing readily available VR hardware and software towards virtual outcrop data interpretation, we can provide the community with immediate access to virtual reality analytical tools capable of producing geologically meaningful outputs. In turn, we hope that the proof of concept study presented here and the VR data processing pipeline provided herein will provide the virtual outcrop community with tools through which the utility of VR interface technologies can be evaluated, without the need for the time consuming development of bespoke digital outcrop focused analytical software with VR user interface support.

We demonstrate the power of the approach by digitizing and analyzing cataclastic fault systems (shear bands) from exposures of the Permian aged Penrith Sandstone formation (Vale of Eden Basin) within Lacy’s Caves, northwest England. For validation, 3D trace maps generated using consumer grade VR hardware and software tools presented here are compared to two equivalent datasets: one interpreted through manual polyline interpretation on a flat panel display using OpenPlot (Tavani et al., 2011), and another extracted using optical ray tracing (Seers and Hodgetts, 2016b). Finally, prospects for the adoption of VR based immersive visualization strategies within digital outcrop data analysis, as well as for the wider geosciences are also discussed.

## 2. Materials and methods

In this section, VR hardware and software specifications, as well as data collection, post-processing and analysis procedures for the interpretation of digital outcrop datasets using consumer grade virtual reality hardware and software are described in detail. We have provided a comprehensive code library written in the MATLAB™ language through

which the results of this study can be replicated (a description of the functionality of the component Matlab files is provided in Table 1). The functionality of OpenPlot is not described in detail in this section, as this has been presented elsewhere (e.g. Stefano et al., 2011; Tavani et al., 2019; Corradetti et al., 2017). However, aspects of basic functionality are provided in Section 3.1.

### 2.1. Hardware

We utilize a widely available consumer grade VR system (HTC Vive) to digitize geological structure from digital outcrop models within this study (Fig. 1a). The HTC Vive consists of a VR headset containing dual screen 1080 × 1200-pixel resolution (2160 × 1200 combined) organic light-emitting diode (OLED) display providing 90 Hz refresh rate and 110° field of view. The system is also equipped with two hand-held motion controllers which enable the operator both to interact with their virtual surroundings and operate the user interface of software displayed through the Vive’s paired screens. A pair of pulsed infrared (IR) laser imitating base stations provide the principle means of tracking

**Table 1**

Matlab VR processing pipeline code library (tested on Matlab, 2017a). Code authored by T. D. Seers unless otherwise indicated.

File	Description
<i>modTransform.m</i>	(Script) Performs a similarity transform to spatially rectify Google Tiltbrush generated patches (see Section 2.3)
<i>schmidt.m</i>	(Script) Generates a Schmidt net equal area projection (authored by Gerry Middleton)
<i>tiltbrush_script.m</i>	(Script) Used to deploy the mesh postprocessing pipeline for Tilt Brush generated mesh patches
<i>absorQuart.m</i>	(Function) Implementation of Horn’s Method for the solution to the absolute orientation problem
<i>arealDensityNoSet.m</i>	(Function) Calculates an areal fracture intensity map ( $P_{21}$ ) using 3D discontinuity traces and an outcrop model triangulated mesh (see Fig. 10)
<i>colPlyExport.m</i>	(Function) Exports a colored point cloud in the Stanford Polygon format (.ply)
<i>curveSort.m</i>	(Function) Sorts the vertex list of 3D traces extracted from Tilt Brush generated mesh patches by nearest neighbors (see Fig. 4/Algorithm 1)
<i>inertia.m</i>	(Function) Eigen solution to the least squares plane problem
<i>lineDist.m</i>	(Function) Calculates the length of 3D line segments
<i>lineDistSq.m</i>	(Function) Calculates the length of 3D line segments (squared distance)
<i>mesh_load.m</i>	(Function) Mesh import (.ply format): no color
<i>meshLoad_col.m</i>	(Function) Mesh import (.ply format): vertex color
<i>mesh2meshGPU.m</i>	(Function) Finds the curve of intersection between to triangulated meshes (requires a CUDA enabled graphics processing unit)
<i>meshArea.m</i>	(Function) Calculates the area of a triangulated mesh
<i>meshCol_export</i>	(Function) Exports a triangulated mesh in the Stanford Polygon format (.ply): vertex color
<i>meshCol_Face_export.m</i>	(Function) Exports a triangulated mesh in the Stanford Polygon format (.ply): face color
<i>meshDense.m</i>	(Function) Mesh vertex densification (face splitting)
<i>meshGPU.m</i>	(Function) Setup of the GPU array object (see <i>mesh2meshGPU.m</i> )
<i>prop2cols.m</i>	(Function) Converts scalar properties to 8-bit red-green-blue color vectors (using Matlab’s <i>Jet colormap</i> )
<i>rayTriGPU.m</i>	(Function)
<i>simpleMeshExport.m</i>	(Function) Exports a triangulated mesh in the Stanford Polygon format (.ply): no color
<i>splitFV.m</i>	(Function) Splits a mesh into disconnected components (authored by Sven Holcombe)
<i>vect2dip.m</i>	(Function) Converts a directional cosine into dip and dip azimuth
<i>Duct_Tape_Trans.ply</i>	(Data) Tilt Brush generated mesh patches in Stanford Polygon format (.ply: see Fig. 2a)
<i>Lacys_Edit.ply</i>	(Data) Lacy’s Caves outcrop model in Stanford Polygon format (.ply: see Fig. 2a)
<i>readme.txt</i>	(Help file) Instructions for running the Tilt Brush VR data post processing pipeline using the provided test data (see <i>Duct_Tape_Trans.ply</i> and <i>Lacys_Edit.ply</i> )

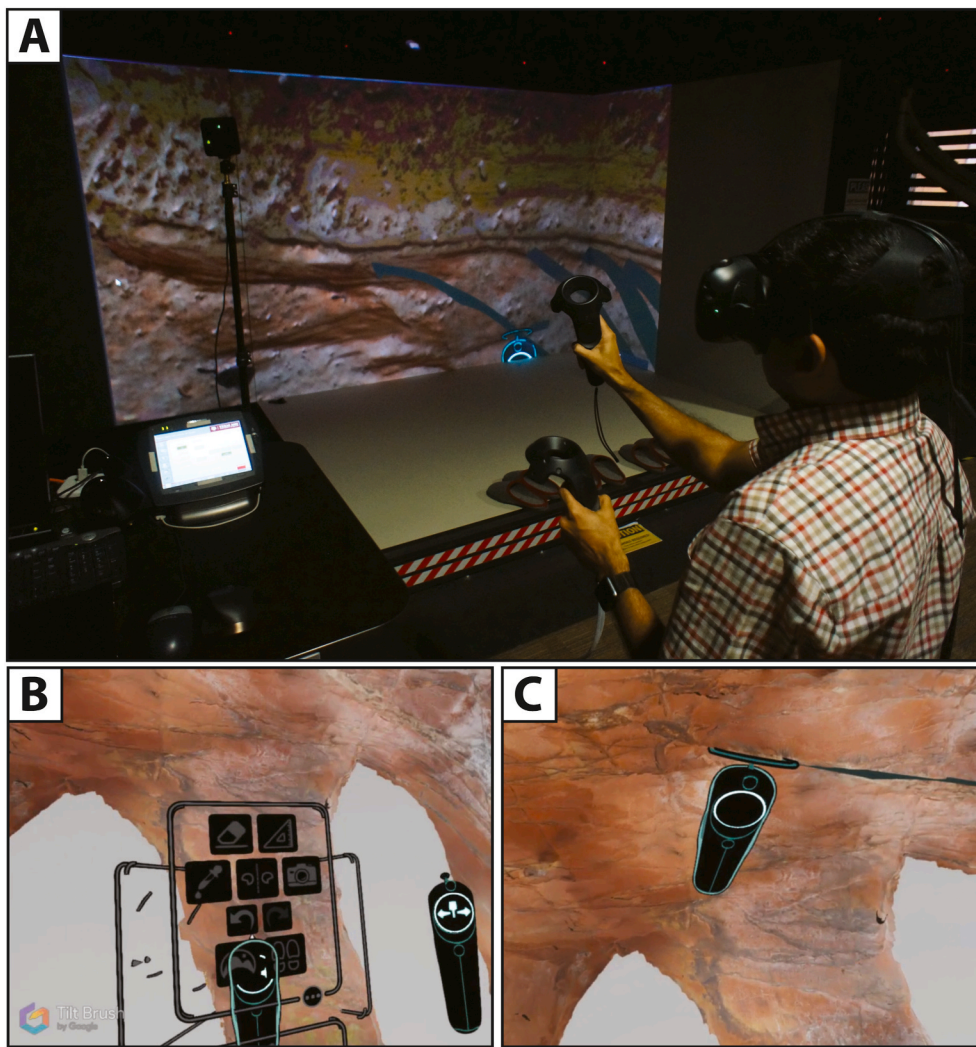


**Fig. 1.** (A) HTC Vive VR system operated within the CAVE immersive visualization center at Texas A&M University at Qatar. In this example, the CAVE system is used for demonstration purposes only, with the interface of the HTC Vive visualized on the CAVE's display panels. (B) Digital outcrop interpretation (photo-textured mesh of Lacy's Caves, NW England) using Google Tilt Brush with virtual palette displayed. (C) Digitization of geologic structures (sandstone hosted shear bands) by manually fitting Tilt Brush generated mesh patches through the outcrop model surface using the Vive's hand-held motion controllers.

the movement of the operator, which are used to detect an array of IR sensors integrated into the headset and motion controller. This tracking system provides a  $360^\circ \sim 4.5 \times 4.5$  m virtual workspace in which the Vive can be operated. IR sensors are supplemented by additional gyroscope, inertial and proximity sensors located within the Vive's headset.

## 2.2. Software

In this study, digitization of geological structures from outcrop models is conducted using Tilt Brush: a VR ready freeform digital arts software package developed Google. When utilized with a supported virtual reality hardware platform (i.e. HTC Vive, Oculus Rift), Tilt Brush facilitates the creation of room-scale 3D artwork, with brush strokes produced using handheld VR motion controllers represented as mesh patches. Brush style, size and color selection, as well as import/export routines are accessed via a 'virtual palette' (Fig. 1b), with options selected using the Vive's handheld motion controllers.

A critical feature of this software platform pertinent to the present work is support for import of textured/RGB colored triangular meshes saved as Wavefront. obj format. This functionality enables digital outcrop models to be visualized and interpreted using Tilt Brush's VR graphics creation toolset. It should be noted that, unlike conventional 3D mesh/point cloud viewers (e.g. Meshlab, Cloud Compare, Virtual Reality Geological Studio: Cignoni et al., 2008; Girardeau-Montaut, 2015; Hodgetts, 2013) which continuously transform the viewport to achieve the users desired world coordinate window, models input into

Tilt Brush must first be manually transformed by the operator using handheld motion controllers to their desired orientation and scale with respect to the virtual workspaces reference frame. Consequently, a spatial (roto-scaling-translation) transform must be applied to models and interpretations output from Tilt Brush in order to revert them back to input model's antecedent registration scheme (see Section 2.3).

The reader should note that Tilt Brush does not provide any user interaction or feedback with the imported mesh other than the spatial transforms alluded to above, meaning that it is not possible to fit polylines directly to the outcrop model surface. To obtain such data, mesh patches are fitted locally through the geologic discontinuity of interest approximately perpendicular to the outcrop surface (Fig. 1c). Geological traces digitized as polylines are then extracted by finding the intersection between Tilt Brush fitted mesh patches and the outcrop model surface during post-processing. In this study, we use Tilt Brush's 'Duct Tape' brush style, which produces simple planar mesh patches (Fig. 2a), to map targeted geologic structures. Due to the nature of the proposed 3D trace extraction procedure, it is important at this stage to set the width of the brush such that the fitted patch fully intersects the mesh along the length of the mapped discontinuity. Manually fitted mesh patches, as well as the transformed outcrop model may be exported as triangular meshes in. obj format, with the spatial transform required to map these outputs back to the registration scheme of the original input model exported as Filmbox (.fbx) graphics exchange format.

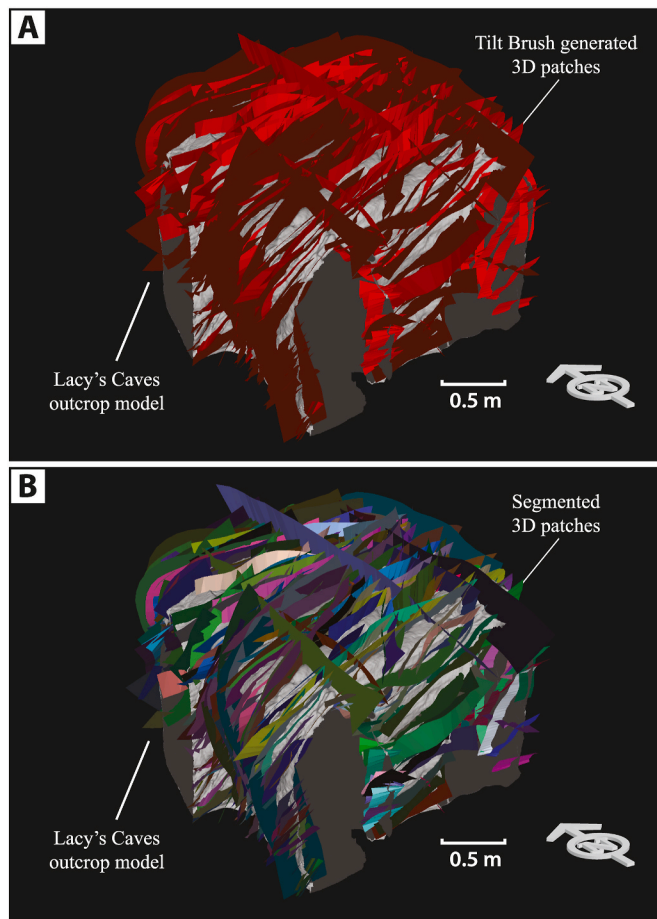


**Fig. 2.** (A) Tilt Brush generated mesh patches fitted to 275 shear bands identified from the Lacy's Caves outcrop model. Interpretations were conducted by a single operator and took approximately 100 min to complete. A video documenting import and interpretation of 3D outcrop models using Tilt Brush is available in the *supplementary materials*. (B) Tilt Brush exported brush strokes output as a single mesh are segmented into individual mesh patches.

### 2.3. Post processing

Google Tilt Brush's intended application as a visual arts software tool means that it effectively contains null functionality for data analysis. Consequently, we have developed a processing pipeline developed in the MATLAB language (available in supplementary materials) capable of extracting structural traces/geological contacts and statistical data from Tilt Brush generated 3D patches. As a pre-processing step, it is necessary to rectify the outcrop model output from Tilt Brush with its corresponding camera transform (output as .fbx format). In this study, 3DS

Max, a commercially available 3D modeling, animation, rendering, and visualization software package developed by Autodesk is used to apply this transform, though open-source software with equivalent functionality may also be used (i.e. Blender). Considering a subsample from the vertex list of the Tilt Brush transformed outcrop model and their analogue vertices from the original outcrop model, the required transformation matrix can then be calculated from these matched point sets by solving the absolute orientation problem using Horn's unit Quaternion-based closed form method (Horn, 1987). Applying this transform to the Tilt Brush output patches corrects modifications in

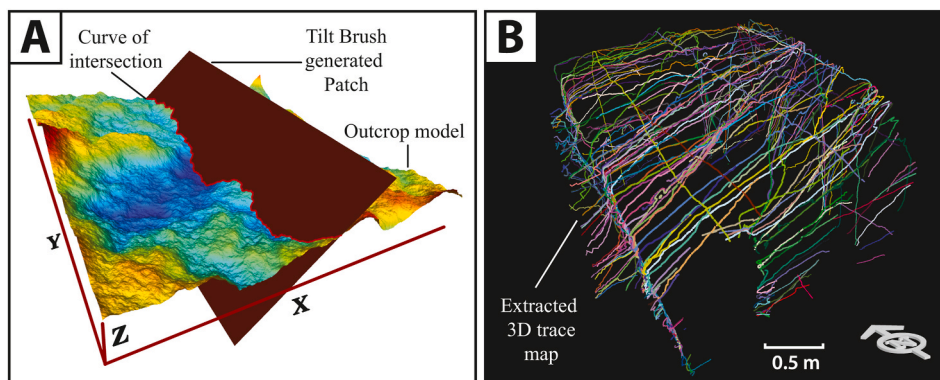


**Fig. 3.** (A) Geologic traces are extracted from Tilt Brush generated patches and the mapped 3D outcrop model using the mesh-mesh intersection algorithm of Seers and Hodgetts (2016). (B) 3D fracture trace map extracted using the patches displayed in Fig. 3.

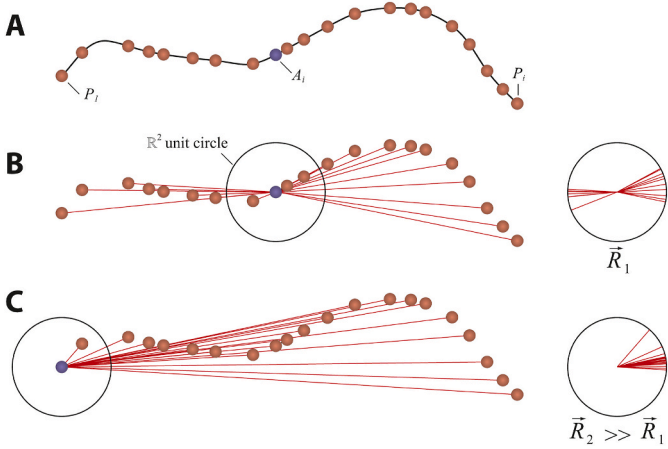


**Fig. 4.** (A) Digitized discontinuity trace segment within a local neighborhood around the point of interest  $A_i$ , represented by unordered, non-uniformly spaced points. (B) Candidate end node,  $A_i$ , is transformed to the origin of the unit sphere (shown as the unit circle for parsimony). This translation vector is subtracted from  $P$ , forming a system of vectors,  $X$ , whose individual magnitudes correspond to the distance between each element of  $P$  and  $A_i$ .  $X$  is normalized, giving a unit vector distribution,  $\hat{X}$ . (C) The trace object's end node equates to  $\hat{X}$  with the resultant vector  $\vec{R}$  with the greatest magnitude (i.e. the vector distribution exhibiting the least dispersion).

scale, orientation and position induced by the user during setup of the virtual workspace (see `modTransform.m` in the supplementary materials).

Contrary to widely used software tools for digital outcrop data analysis presented in Section 2.2, Tilt Brush does not allow user to directly fit polylines onto the outcrop model surface. To harness Tilt Brush for virtual outcrop analysis, the user must fit triangulated mesh patches coincidental to the structures of interest exposed on the outcrop model surface. To obtain useful data for further analysis (i.e. traces represented as polylines), it is necessary to extract the curve of intersection between manually fitted Tilt Brush patches and the outcrop model triangulated mesh. It should also be noted that mesh patches exported from Tilt Brush are output as a single mesh object, precluding the analysis of individual geologic features mapped using its virtual workspace. As a consequence, it is necessary to segment the face list of the Tilt Brush mesh into individual mesh patches (Fig. 2b), using connected components analysis. Subsequently, 3D mesh patches and their parent outcrop model are used as the basis for geologic trace extraction,

utilizing a hardware accelerated implementation of the mesh-mesh intersection algorithm of Seers and Hodgetts (2016b)/Fig. 3. The aforementioned method utilizes a brute force search of the intersecting mesh face indices, with individual intersections being located by assuming that each triangle edge is an infinitesimal ray, then solving the ray-triangle intersection problem using the classic solution of Möller and Trumbore (1997). Positive intersections are detected when the intersecting point,  $p_0$  lies in-between the end nodes of its associated triangle edge ( $p_1, p_2$ ), determinable via the following criterion

$$\|p_0 - p_1\| + \|p_0 - p_2\| = \|p_1 - p_2\| \quad 1$$

The brute force approach described above results in the trace of intersection being extracted in the form of an unsorted vertex list. However, it is necessary to establish nearest neighbor relationships between individual points, in order to extract key metric data (esp. fracture trace length and intensity) from the VR digitized 3D trace map. Establishing such relationships is a non-trivial undertaking, particularly as trace point sets are output with non-uniform spacing and correspond to a non-parametric curve of intersection, (i.e. created by a geologic discontinuity and the outcrop), precluding the use of parametric curve fitting.

It is first necessary to locate one end node of a trace's point set. Identifying end nodes of a trace can be achieved via brute force, though the use of a naive search strategy is unattractive, due to large run times for datasets of many hundreds to thousands of traces. Thus, we isolate potential candidates through the use of a moving window based approach. A local neighborhood is constructed around each point of interest,  $A_i = \{x_i, y_i, z_i\}$ . We assume  $A_i$  and its neighboring vertices,  $P = \{p_1, p_2, \dots, p_n\}$  form a vector distribution (noting that  $A_i \notin P$ ), with  $A_i$  corresponding to the origin of an  $\mathbb{R}^3$  unit sphere (Fig. 4a). Assuming null duplication in the trace objects point list,  $P$  forms  $n$  unique vectors [ $X = X_1, X_2, \dots, X_n$ ], with magnitudes equating to the distances between  $A_i$  and the elements of  $P$ , which are normalized to form the unit vector distribution  $\hat{X}$  (whereby  $\hat{X}_i = \frac{X_i}{|X_i|}$  and where  $|X_i|$  is the norm of  $X_i$ ; Fig. 4b). We assume that the true end node of the trace's point set,  $A_{min}$ , approximating to the termination of its parent discontinuity, corresponds to the unit vector distribution ( $\hat{X}_1, \hat{X}_2, \dots, \hat{X}_k$ ) where the (square) magnitude  $R$  of the resultant vector,  $\vec{R}$ , is maximized (Fig. 4c)

$$A_{min} \hat{=} \max\{R_1, R_2, \dots, R_k\} \quad 2$$

where

$$R_k = n + 2 \sum_{i=1}^n \sum_{j=1, j \neq i}^n \hat{X}_i \cdot \hat{X}_j \quad 3$$

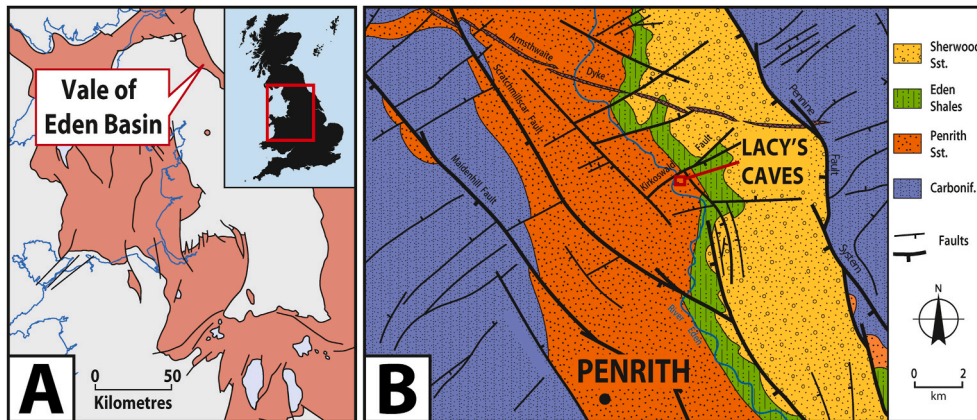


**Fig. 5.** (A) Permo-Triassic outcrop for central and northern England and Wales, with current study area (Vale of Eden Basin) indicated. (B) Central portion of the Vale of Eden Basin, with the location of Lacy's Caves indicated. Reproduced from Seers and Hodgetts (2016b)/(A adapted from Mountney and Thompson, 2002/B redrawn from Fowles and Burley, 1994).

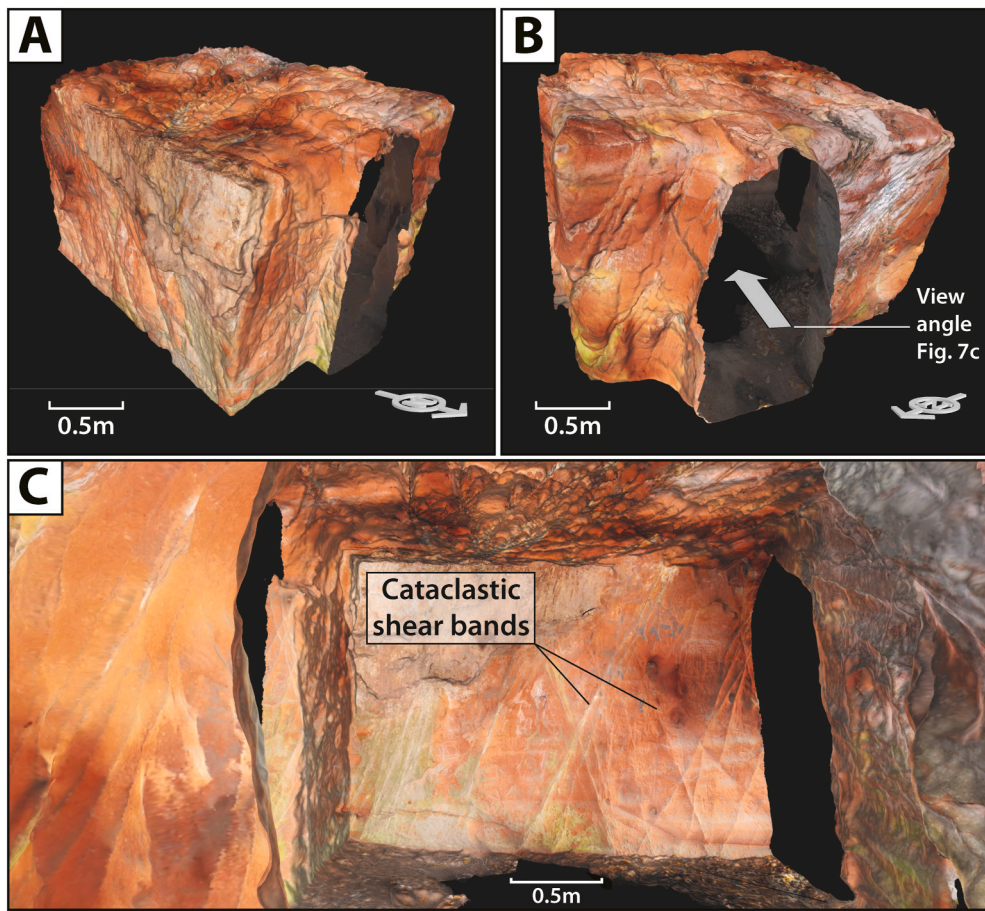


**Fig. 6.** (A–C) Different views of a textured triangular irregular mesh-based surface model of the Lacy’s Caves outcrop constructed from a structure from motion estimation–multi-view stereo (SfM-MVS)–derived point cloud using the Poisson surface reconstruction algorithm. Reproduced from [Seers and Hodgetts \(2016b\)](#).

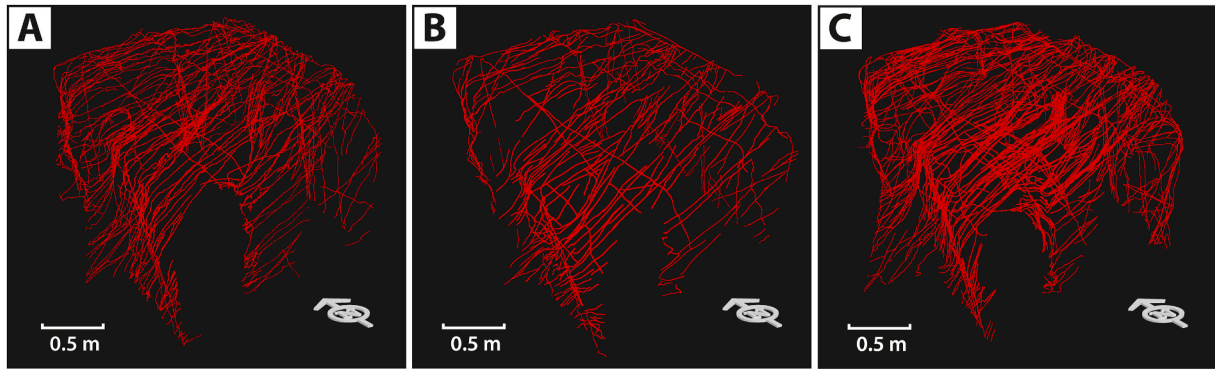


**Fig. 7.** 3D fault trace maps extracted from the Lacy’s Caves outcrop model using (A) the VR based workflow presented here, (B) the polylines extracted in OpenPlot and (C) the optical raytracing based approach of [Seers and Hodgetts \(2016a\)](#).

whereby  $\hat{X}_i \cdot \hat{X}_j$  is the scalar product of  $\hat{X}_i$  and  $\hat{X}_j$  such that  $\hat{X}_i \cdot \hat{X}_j = (\hat{x}_i \cdot \hat{x}_j + \hat{y}_i \cdot \hat{y}_j + \hat{z}_i \cdot \hat{z}_j)$ , and where  $\hat{x}_i, \hat{y}_i, \hat{z}_i$  and  $\hat{x}_j, \hat{y}_j, \hat{z}_j$  are the cartesian vector components of  $\hat{X}_i$  and  $\hat{X}_j$  respectively. Thus, maximizing  $R$  corresponds to the maximization of the sum of the scalar products of  $\hat{X}_i$  and  $\hat{X}_j$ , whereby higher sums will equate to more positively collinear vectors

(i.e. produced by the extracted trace features’ end nodes: [Fig. 4c](#)).

Having identified the trace object’s end node, the remaining point set is sorted via a (naive) nearest neighbor search. We employ a user defined threshold of maximum vertex separation to isolate potential degenerate cases output from the sorting procedure outline above. In such cases, the end nodes are identified via a brute force search. A pseudocode summary of the line sorting routine is as follows:

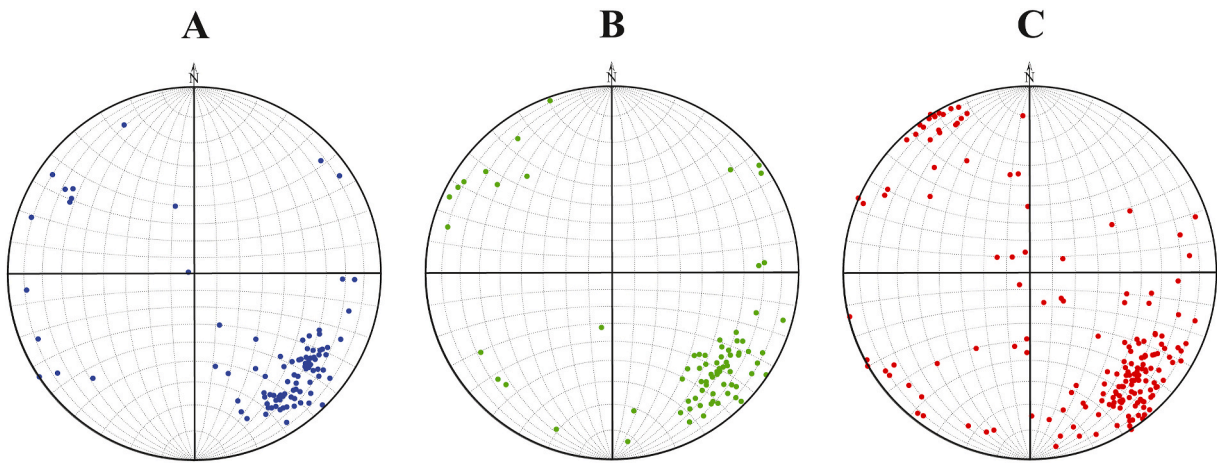


**Fig. 8.** Lower hemisphere, stereographic equal-area projections of poles to fault planes for (A) VR digitized, (B) OpenPlot digitized and (C) optical raytracing extracted 3D trace maps.

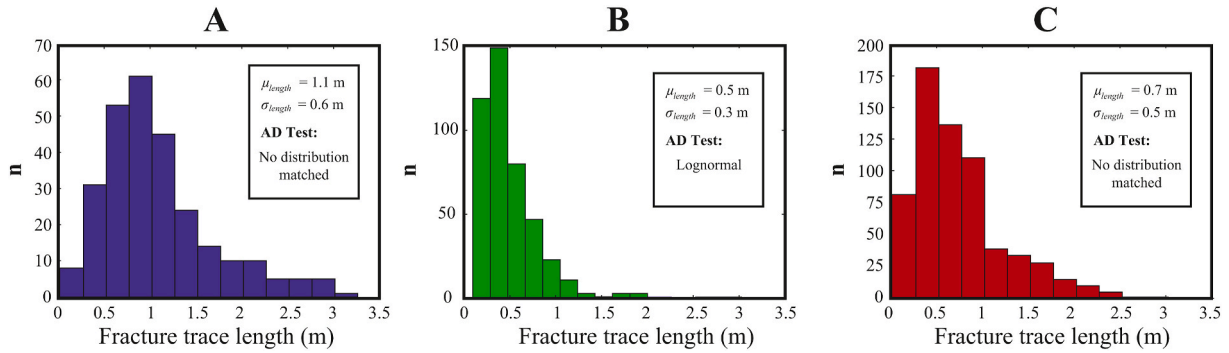


**Fig. 9.** Fault trace length distributions for (A) VR digitized, (B) OpenPlot digitized and (C) optical raytracing extracted 3D trace maps. Note that the Anderson-Darling test results displayed in Fig. 9 are in the format equivalent to Matlab figures output by the presented VR processing pipeline.

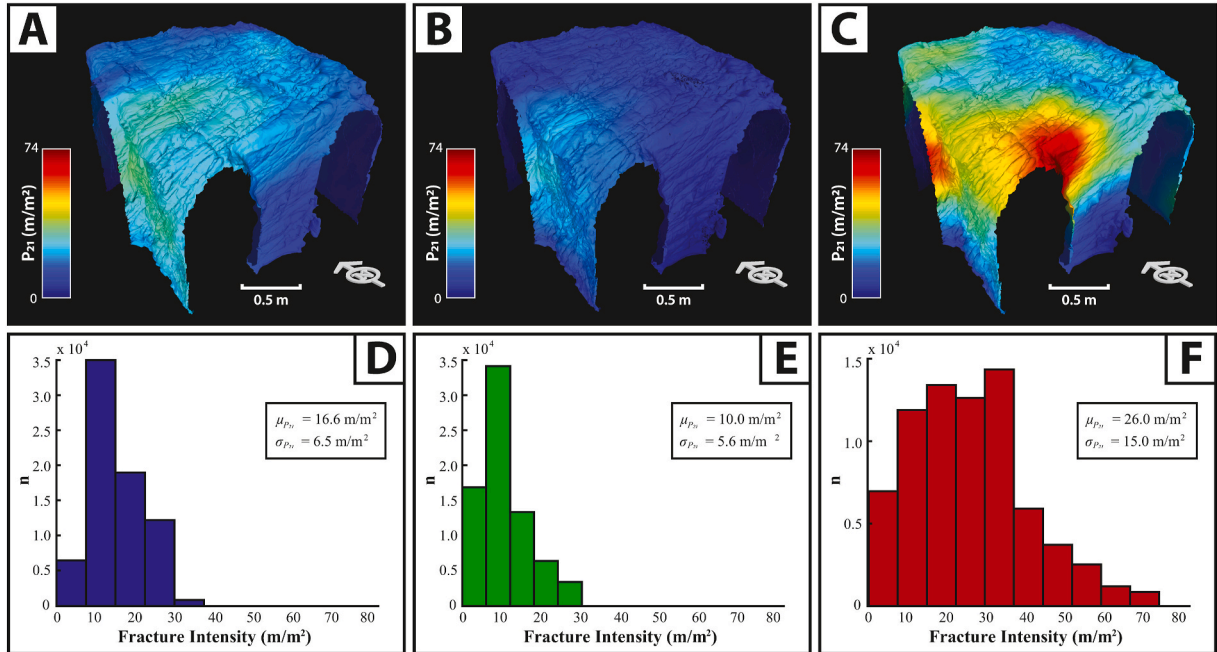


**Fig. 10.** Areal fault intensity ( $P_{21}$ ) vertex attribute maps for (A) VR digitized and (B), OpenPlot digitized and (C) optical raytracing extracted 3D trace maps.  $P_{21}$  frequency distributions for (D) VR digitized, (E) OpenPlot digitized and (F) optical raytracing extracted 3D trace maps.

---

**Algorithm 1:** curveSort

---

**function** CURVESORT( $T, \epsilon$ )

▷  $T$  contains unsorted trace vertices as row vectors ( $m \times 3$ )

▷  $\epsilon$  is a scalar which defines the radius of the spherical neighborhood

▷  $T_{\text{sort}}$  (OUTPUT) contains sorted trace vertices as row vectors ( $m \times 3$ )

**for** number of rows in  $T$  **do**

▷ Sort initialization: locate  $A_{\min}$

$A_i \leftarrow i^{\text{th}}$  row of  $T$

$T_i \leftarrow$  **delete**  $i^{\text{th}}$  row of  $T$

$P \leftarrow (A_i^2 - T_i^2) < \epsilon^2$

$\hat{X}_i \leftarrow \frac{P - A_i}{|P - A_i|}$

$R_i \leftarrow$  **sum**( $\hat{X}_i$ )

$A_{\min} \triangleq \mathbf{max}\{R_1, R_2, \dots, R_k\}$

▷ Initialize nearest neighbor search

$S \leftarrow A_{\min}$

$Q \leftarrow$  **delete** row  $T(j)$  where  $T(j) \triangleq S$

$T_{\text{sort}} \leftarrow S$

**for** number of rows in  $Q$  **do**

▷ Nearest neighbor search

$d \leftarrow$  compute **distance**( $S, Q$ )

$I \leftarrow$  find index **min**( $d$ )

$S \leftarrow Q(I)$

**append**( $T_{\text{sort}}, S$ )

**delete** row  $Q(I)$

**return**  $T_{\text{sort}}$

---

It should be noted that vertex sorting can be an intractable problem in cases where trace geometry is strongly overturned (i.e. fracture traces mapped within caves or tunnels), meaning that the strategy outlined above cannot be considered universally robust. The user should note that the approach is sensitive to mesh artifacts (esp. anomalous disconnected mesh patches typically arising from surface reconstructions of noisy point clouds), which produce false points of intersection during the previously described trace extraction procedure. Mesh patches displaying regions of low vertex density may also reduce the reliability of vertex sorting (note that a mesh densification function to address such issues is available in the *supplementary materials* section: see meshDense.m). Thus, it is important for the user to quality check the input mesh used for 3D trace extraction, with several free and/or open source software packages being available for point cloud and mesh filtering and cleaning (e.g. Meshlab, Blender, Cloud Compare).

Potentially, more robust results could be obtained by explicitly using mesh topology (i.e. via the mesh face indices). In this scenario intersection testing would be conducted iteratively, whereby neighboring triangles are located and tested within a region growing framework, providing native line tracking and vertex sorting during extraction. Despite these caveats, we find that the procedure was sufficiently accurate to sort the point lists of the 3D traces generated in the test case presented in Section 3 (mapped from Lacy's Caves, NW England). Moreover, we consider the approach performance-wise to be acceptable, with intersections between individual Tilt Brush fitted fracture patches (mean faces per patch:  $\sim 90$ ) and the Lacy' Caves outcrop model ( $\sim 146000$  faces) presented in the preceding section being solved (on average) in less than 1 s using an Intel i7-7700HQ CPU with 32 GB RAM and a GTX 1070 GPU.

The 3D trace map output from the workflow outlined above and its

accompanying outcrop model forms the basis for the extraction of statistical data (trace length, orientation, fracture/fault density). Analytical procedures for the extraction of discontinuity statistical data from VR generated trace maps are detailed in the following section.

## 2.4. Analysis

Seers and Hodgetts (2016b) demonstrated the potential of 3D fracture/fault datasets as an analytical medium for the extraction of discontinuity statistical data. 3D fracture trace maps obtained from Tilt Brush generated patches are amenable to the same analytical routines applied to equivalent datasets generated using alternate methods (e.g. using photogrammetrically calibrated images, orthorectified images and digital elevation models, mesh curvature: Seers and Hodgetts, 2016b; Umili et al., 2013; Vasuki et al., 2014). In this work, we focus on the estimation of trace length statistics (mean, standard deviation, parametric distribution goodness of fit tests), structural orientation (mean vector and estimated concentration parameter of the Fisher-von Mises distribution) and areal intensity vertex property mapping ( $P_{21}/m/m^2$ : Dershowitz and Herda, 1992)/(see Seers and Hodgetts, 2016b for further details of this analysis workflow).

## 3. Application to shear band characterization

To demonstrate the potential of virtual reality based digital outcrop data analysis, we have extracted a three-dimensional fault trace map from exposures of the Permian aged Penrith Sandstone Formation within Lacy’s Caves, Vale of Eden Basin, UK (Fig. 5). The structure from motion-multiview stereo (SfM-MVS) derived textured mesh used within this study (Fig. 6) has previously been utilized by Seers and Hodgetts (2016b) as the basis for 3D trace map extraction using calibrated image sequences (see the aforementioned study for details of the geological setting of the study area and the outcrop model generation procedure). The availability of such a dataset, together with a new interpretation made in OpenPlot facilitates comparison between fault properties from traces extracted using VR based analysis of textured meshes ( $n = 274$ ), flat panel display-based analysis of textured meshes in OpenPlot ( $n = 440$ ) and those calculated from traces generated using effectively lossless state-of-the-art pixel-based analysis of raster imagery ( $n = 645$ )/Fig. 7. Discrepancies between the number of identified faults between the VR, OpenPlot and ray tracing based 3D trace map generation workflows may be attributed to downsampling of input imagery used for texture map generation, which results in the censoring of finer-scale shear bands from the formerly mentioned dataset. In terms of acquisition speed, the VR based dataset was compiled in approximately 100 min, with the OpenPlot dataset requiring 273 min for digitization. The optical ray tracing dataset presented by Seers and Hodgetts (2016a) required over 900 min to compile, due in part to the higher number of identifiable traces, but also because this technique requires manual linkage and merger of traces split between contiguous images (see Seers and Hodgetts, 2016a).

### 3.1. Fault orientation

The estimation of fault/fracture orientation from 3D trace datasets poses challenges, due to the decay of orientation precision as the trace’s vertex list converges towards and deviates away from idealized collinear and coplanar configurations respectively (Seers and Hodgetts, 2016a,b). Consequently, we impose limits on vertex collinearity,  $K$  [ $K = \ln(\lambda_1/\lambda_2)/\ln(\lambda_2/\lambda_3)$ ], and coplanarity,  $M$  [ $M = \ln(\lambda_1/\lambda_3)$ ]/(Fernández, 2005; Woodcock, 1977), where  $\lambda_1$ ,  $\lambda_2$  and  $\lambda_3$  are eigenvalues obtained from principle components analysis (PCA) on the trace’s vertex coordinates. Following the work of Fernández (2005) and Seers and Hodgetts (2016a), we restrict eigensolution based estimation of best fit planes to trace vertex sets where  $K < 1$  and  $M > 4.93$  and 178 3D traces with vertex coplanarity and collinearity values below and above these

thresholds were identified from VR and ray tracing generated 3D trace map datasets respectively. In the OpenPlot workflow (e.g. Corradetti et al., 2017), the issue of collinear trace features is handled in real-time through the live computation of a best-fit plane from pointsets picked from the outcrop model surface across the length of each identified discontinuity trace. Thus, the user has the ability to evaluate the goodness of the derived best-fit plane for each geological feature during the digitization, by setting visual  $K$  and  $M$  threshold values and/or simply by qualitative interpretation. For the sake of comparison, in this study this interpretative evaluation was solely qualitative and the resulting dataset was later processed in accordance with the other obtained datasets.

A comparison between poles to plane orientation estimates obtained from VR, OpenPlot and optical ray tracing generated traces is displayed in Fig. 8 (orientations estimated using  $K < 1$  and  $M > 4$ ). Qualitative comparison orientation distributions are globally equivalent, with two dominant conjugate and steeply dipping NE-SW striking sets readily identifiable from both datasets. A secondary (i.e. less developed) set corresponding to NW-SE striking shear bands can also be confidently identified from the ray tracing extracted dataset. This NW-SE striking set is ambiguous in the VR generated and OpenPlot datasets due to the limited pole vector count after filtering. The optical ray tracing extracted dataset also displays an apparent sub-horizontal set, which relates to the fitting of least squares planes through smaller curvilinear fault traces exposed on the roof of the cave, resulting in measurements that represent the outcrop rather than the target discontinuity orientation (see Seers and Hodgetts, 2016b). Such smaller traces are less identifiable during VR trace interpretation, owing to the limited pixel density of the outcrop model texture maps used in the VR trace and OpenPlot extraction procedures.

### 3.2. Fault trace length

In this study, we define trace length as the chordal distance between the end nodes of a given fault trace. Having determined the lengths of individual fault traces, per orientation set trace length statistics (mean and standard deviation/geometric mean and geometric standard deviation) are calculated for fault traces extracted using virtual reality, OpenPlot and optical ray tracing based analyses (e.g. Biber et al., 2018). Further to this, Anderson-Darling statistical tests (Anderson and Darling, 1954) are used to determine the goodness of fit between the empirical trace length distributions and parametric distributions commonly used to describe fracture trace length (normal, lognormal, exponential, power law: e.g. Baecher et al., 1977; Hatton et al., 1994; La Pointe, 2002; Priest and Hudson, 1981; Priest, 2012). Finally, we utilize the non-parametric Kruskal-Wallis test (Kruskal and Wallis, 1952) to determine whether VR and ray-tracing interpreted, as well as VR and OpenPlot interpreted trace lengths are derived from the same distribution.

A comparison between fault trace length distributions obtained from VR, OpenPlot and optical ray tracing based approaches is displayed in Fig. 9. Despite the previously identified disparities amongst individual trace populations, the presented digitization strategies produce comparable trace length statistics for both clearly identifiable orientation sets (Fig. 9). However, should be noted that the different approaches impacted the mean trace length. For instance, there is clearly a propensity towards mapping larger traces over the textured mesh in the VR approach (Fig. 9a). The real-time user assisted plane computation of OpenPlot (see Section 3.1) during the digitization of the traces resulted in a shorter mean fracture length and the lowest standard deviation of the tested approaches. The digitization of points out of the planar real-time planar interpolation was in fact avoided by the user, provided by the ability to qualitatively estimate if the addition of points that would fall out of the expected interpolation, favoring segmentation (e.g. Tavani et al., 2019). As a consequence, longer curvilinear fractures were broken down during the digitization in OpenPlot. The aforementioned approach also accounts for the disparity in the number of traces digitized by the VR and OpenPlot workflows, which utilized the same input textured

mesh. Trace length distributional forms produced by the compared digitization strategies are ostensibly similar, exhibiting negative skewed distributions (Fig. 9). In two cases (VR and optical ray tracing), Anderson-Darling tests are unable to determine goodness-of-fit between the empirical trace length distributions and the tested parametric forms at the selected alpha value ( $P > 0.05$ ), while in the OpenPlot case a lognormal distribution was recognized. Moreover, Kruskal-Wallis tests reject the null hypothesis that both VR and ray-tracing/OpenPlot generated trace length populations come from the same distribution at a 1% significance level ( $P = 0.033$  and  $P = 0.00001$  for  $n = 30$  random subsamples of from each population).

### 3.3. Areal fault intensity

The value of utilizing 3D discontinuity traces to generate vertex attribute maps of areal fault/fracture intensity (i.e. fracture length per unit area  $m/m^2/P_{21}$  *sensu* Dershowitz and Herda, 1992) has been demonstrated by a number of authors (Pearce et al., 2011; Seers and Hodgetts, 2016a). Following Seers and Hodgetts (2016a), we compute per-vertex values of  $P_{21}$  using a moving spherical kernel (kernel radius = 0.5 m) for VR, OpenPlot and optical ray tracing generated fault traces.

A comparison between areal fault intensity obtained through the different digitization strategies presented herein is displayed in Fig. 10a–c, with distributions of  $P_{21}$  produced by each respective technique displayed in Fig. 10d–f. The spatial distribution of  $P_{21}$  for fault traces generated via the compared digitization techniques is outwardly similar. However, it is noteworthy that fault densities calculated from textured mesh generated traces (i.e. VR and OpenPlot) exhibit markedly lower values than those mapped using optical ray tracing based techniques (see Fig. 10). Again, these disparities relate to resolution dependent censoring of finer traces from the textured mesh dataset used as the analytical medium in the VR based workflow (see Section 3).

## 4. Discussion and conclusion

In this study, we have explored and demonstrated the potential of applying consumer grade virtual reality hardware and software towards the visualization and analysis of digital outcrop datasets. A MATLAB based post-processing pipeline has been presented, which facilitates the extraction of structural traces and bedding plane contacts from triangular mesh patches fitted to digital outcrop model surfaces using VR based interpretation. It is hoped that this work and associated code library will help to accelerate the inclusion of virtual reality based geologic interpretation into existing digital outcrop model analytical workflows, by enabling users to harness a widely adopted VR freeform 3D graphics package (Google Tilt Brush), thus negating the need for time consuming development of bespoke software. Nevertheless, we suggest that as VR based digital outcrop visualization and interpretation techniques mature, such functionality will find inclusion within standalone custom software packages focused upon the analysis of digital outcrop models (e.g. Virtual Reality Geological Studio: Hodgetts, 2013). A potential development route may be to harness existing 3D gaming engines (e.g. Unreal Engine or Unity) which have existing support for virtual, augmented and mixed reality user interface paradigms, as well as the most common graphics primitives used in the visualization of virtual outcrop models (i.e. triangulated irregular networks and texels).

Though the tested application presented here focuses upon the digitization of fault networks from digital outcrop models, VR based interpretation has potentially wide reaching applications within the geosciences. Indeed, our approach may be leveraged towards the interpretation of an array of geological and geomorphological structures (e.g. sedimentary architecture, fold geometry, bedding contacts, glacial lineations: Corradetti et al., 2017; Labourdette and Jones, 2007; McCormack et al., 2008) from close range 3D remote sensing datasets. Furthermore, the VR based digitization workflow presented here may also be appropriated towards the interpretation of geologic structure

from datasets captured using airborne or space-borne sensors (i.e. radar or lidar altimetry data: e.g. Masoud and Koike, 2006), or even used to digitize features of interest from geophysical survey or lab-based image data (i.e. seismic sections, ground penetrating radar transects or orthoslices from tomographic images: e.g. Lister, 2004; Voorn et al., 2015), with the only constraint being that the analyzed data is represented as a 3D textured mesh.

In the case study presented in Section 3, virtual reality based fracture characterization was capable of producing datasets broadly equivalent to those generated using OpenPlot and optical ray-tracing, against which it was benchmarked. Though there are clear disparities between the aforementioned datasets in terms of mappable structures, such differences can be viewed as synthetic, being a product of the pixel density of the outcrop model texture map used in the VR analysis workflow. These effects are attributable to resolution dependent statistical truncation of the fracture trace datasets, as recognized by Sturzenegger et al. (2007). Such differences may be partially abated by the use of higher resolution textures within the VR outcrop model analysis routine. There are additional factors that can be deleterious to feature detection from textured meshes. In addition to texture resolution, the quality of the input images for texture generation must also be considered, with motion blur, low signal-to-noise characteristics (i.e. due to the use of high ISO camera settings during field acquisition) and the selection of texture compression procedure being detrimental to texture fidelity, and in the case of stereo-photogrammetry, negatively impactful upon the geometry of the reconstructed scene (e.g. Cheng and Bischof, 2006; Han et al., 2014; Vollgger and Cruden, 2016). Moreover, it has been demonstrated that independent of texel density, mesh vertex spacing has a significant impact upon the perceptual quality of triangulated irregular network representations of 3D objects (e.g. Cheng et al., 2006), with the selection of illumination rendering scheme (i.e. direct vs. oblique illumination) coupled with the relative rugosity of the visualized mesh also influential upon perceived object quality (Rushmeier et al., 2000). Conversely, disparities between VR and OpenPlot is directly attributable to the different methodological approaches (i.e. mesh patch fitting using VR controllers and headset vs. polyline fitting using a mouse and flat panel display), given that the input datasets are identical.

In this comparative study, the VR based routine proved more efficient in terms of digitization speed than the raytracing workflow, as it negated the need for time consuming merger of traces from contiguous images (see Seers and Hodgetts, 2016a). Compared to the flat panel display interpretation performed in OpenPlot, the two methods have shown comparable speeds when carried out by competent operators. One tangible advantage of VR digital outcrop interpretation observed in this study was that the Tilt Brush graphical user interface does not suffer issues with the limit of the viewport cut point. This makes the visualization of meshes representing enclosed spaces with multiple parallel walls (i.e. mine workings and caves) challenging in many 3D object viewers. Due to this limitation, it was necessary to conduct the OpenPlot interpretation of the textured mesh from the exterior of the cave. This may be advantageous in cases where the exposure morphology is highly complex, whereby the VR based environment can be leveraged to obtain a more favorable vantage point from which outcrop surface can be interpreted.

It is important to point out that VR analysis does carry several practical limitations when compared to the analysis of digital outcrops using flat panel displays. In terms of convenience, the hardware used in this study is relatively cumbersome, requiring an open clear space for setup and operation. Because the user has either limited or null awareness of their real-world surroundings during operation, there is an elevated chance of injury through unintended collision with objects in their immediate vicinity. The operation of VR interfaces is also typically more physically involved than interaction with conventional flat panel displays, which may result in physical fatigue (Jerald, 2015) and may restrict access for operators with limited mobility. Some users may experience motion sickness during the operation of VR systems (i.e.

simulator sickness/cybersickness)/(Jerald, 2015; Munafo et al., 2017; Tyrrell et al., 2018), which may persist several minutes to hours after usage. It was notable during the execution of the present study that, due to its native resolution and proximity to the user's eyes, the viewports of the tested VR device exhibited significant pixilation during usage, which we felt detracted from the user experience. Improved resolution VR headsets have since become available (e.g. the HTC Vive Pro) which reduce such aliasing effects.

It has been argued by previous workers that VR analysis provides an enhanced user experience over that obtained from flat panel displays, being more spatially cognizant and intuitive than these more conventional interface technologies (e.g. Zhang, 2017). Though empirically backed, other benchmarking efforts have detected only nominal improvements in task performance, when comparing head mounted VR displays to conventional flat panel displays (Stevens and Kincaid, 2015). Such studies were conducted in the context of the application of VR to professional training scenarios, and can offer only generic insights into the potential advantages and limitations of VR environments in terms of user experience and performance. The computer graphics literature is comparatively rich with perceptual benchmarking and analysis studies of mesh quality conditional upon mesh and texture resolution, mesh and texture noise or distortion characteristics, and the selected lighting of the scene (Cheng and Bischof, 2006; Cheng et al., 2006; Dong et al., 2015; Han et al., 2014; Kottayil et al., 2018; Rushmeier et al., 2000; Wang et al., 2012). More recently, there have been attempts to evaluate the perceptual quality of consumer grade VR systems, such as those used in the present study, in order to assess their suitability towards applications that go beyond their initial remit as user interfaces for entertainment devices (i.e. as task simulators for training and rehabilitation applications: see Chessa et al., 2019). Currently, there is, however, a lack of empirically robust perceptual benchmarking studies, which pit emerging interface technologies, such as virtual reality against more accepted visualization technologies for the purpose of digital outcrop analysis, or relatable geoscience applications. Indeed, assessing the perceived quality of remotely sensed outcrop datasets has unique conceptual and technical challenges. For example, geologic structures arguably lack the predictability of expression seen in common man-made objects used in most perceptual benchmarking studies within the computer graphics literature. This ambiguity of expression can lead to the introduction of significant user bias during the interpretation (e.g. Long et al., 2019), implying that achieving a perceptual baseline for such datasets might be challenging. The fact that outcrop datasets are not captured under controlled conditions further complicates the endeavor of building objective perceptual benchmarking studies under controlled conditions using virtual outcrop datasets, with textures commonly displaying shadowing and blur, and meshes potentially suffering occlusions, ranging errors and major variations in vertex density (Sturzenegger and Stead, 2009; Sturzenegger et al., 2007; Vollgger and Cruden, 2016). Finally, the common requirement for geoscientists to observe heterogeneities in outcrop at multiple scales (i.e. centimeter to decameter and beyond), coupled with the computational overhead of operating VR user interfaces with large textures or vertex counts (e.g. Lyu et al., 2019) offers further challenges in terms of latency. To capture heterogeneities at multiple length scales such that VR user experiences approach those of the field, it is clear that visualizations using locally varying texture resolution and/or vertex densities (e.g. adaptive texturing and adaptive mesh refinement: Boubekeur and Schlick, 2008; Kraus and Ertl, 2002) are desirable within geologically focused VR software tools. Despite these highlighted challenges, the development of geologically focused human-computer interaction studies would significantly aid the evaluation of emerging visualization paradigms for the interrogation and analysis of virtual outcrop datasets. It is hoped that the present study and its associated code library may aid the community in undertaking such an assessment by providing non-specialists in virtual reality technology with readily accessible VR analytical tools.

## Code availability

The code library described in this article, as well as test data (Lacy's Caves outcrop model and associated Google Tilt Brush generated mesh patch data) and presentation (.ppt) with videoed examples of Tilt Brush data input and interpretation are available via Mendeley Data: <https://data.mendeley.com/datasets/5w2k48mht7/draft?a=37e896ca-b745-49fc-9ad7-7ede3aaea888>

## Author contributions

Thomas Seers initiated the concept, implemented the code libraries, conducted the outcrop interpretation/analysis, and prepared the manuscript. Ali Sheharyar setup and operated the Vive the CAVE visualization systems, conducted pre-processing operations in 3DS Max and contributed technical input towards manuscript preparation. Amerigo Corradetti performed the comparative interpretation in OpenPlot, contributed to data analysis and manuscript development. Stefano Tavani contributed to data interpretation and manuscript development.

## Declaration of competing interest

The authors declare that they have no known competing financial interests or personal relationships that could have appeared to influence the work reported in this paper.

## Acknowledgements

The financial assistance of Qatar Foundation, the Qatar National Research Fund (NPRP10-0104-170104), Texas Engineering Experimental Station and Total E&P are gratefully acknowledged by the authors. The authors would also like to thank the three anonymous reviewers whose insightful comments and suggestions helped to improve this manuscript.

## References

- Anderson, T.W., Darling, D.A., 1954. A test of goodness of fit. *J. Am. Stat. Assoc.* 49, 765–769.
- Baecher, G., Lanney, N., Einstein, H., 1977. *Statistical Description of Rock Properties and Sampling*, the 18th US Symposium on Rock Mechanics (USRMS). American Rock Mechanics Association.
- Barnes, R., Gupta, S., Traxler, C., Ortner, T., Bauer, A., Hesina, G., Paar, G., Huber, B., Juhart, K., Fritz, L., 2018. Geological analysis of Martian rover-derived digital outcrop models using the 3-D visualization tool, Planetary Robotics 3-D Viewer—Pro3D. *Earth and Space Science* 5, 285–307.
- Biber, K., Khan, S.D., Seers, T.D., Sarmiento, S., Lakshminantha, M., 2018. Quantitative characterization of a naturally fractured reservoir analog using a hybrid lidar-gigapixel imaging approach. *Geosphere* 14 (2), 710–730.
- Boghossian, A.L., Pratt, M.J., Becker, M.K., Cordero, S.I., Dhakal, T., Kingslake, J., Locke, C.D., Tinto, K.J., Bell, R.E., 2019. Inside the ice shelf: using augmented reality to visualise 3D lidar and radar data of Antarctica. *Photogramm. Rec.* 34, 346–364.
- Boubekeur, T., Schlick, C., 2008. A Flexible Kernel for Adaptive Mesh Refinement on GPU. *Computer Graphics Forum*. Wiley Online Library, pp. 102–113.
- Caravaca, G., Le Mouélic, S., Mangold, N., L'Haridon, J., Le Deit, L., Massé, M., 2019. 3D digital outcrop model reconstruction of the Kimberley outcrop (Gale crater, Mars) and its integration into Virtual Reality for simulated geological analysis. *Planet. Space Sci.* 104808.
- Cheng, I., Bischof, W.F., 2006. A Perceptual Approach to Texture Scaling Based on Human Computer Interaction, Eurographics (Short Presentations), pp. 49–52. Citeseer.
- Cheng, I., Shen, R., Yang, X.-D., Boulanger, P., 2006. Perceptual Analysis of Level-Of-Detail: the JND Approach. *IEEE*, pp. 533–540. Eighth IEEE International Symposium on Multimedia (ISM'06).
- Chessa, M., Maiello, G., Borsari, A., Bex, P.J., 2019. The perceptual quality of the oculus rift for immersive virtual reality. *Hum. Comput. Interact.* 34, 51–82.
- Cignoni, P., Callieri, M., Corsini, M., Dellepiane, M., Ganovelli, F., Ranzuglia, G., 2008. Meshlab: an Open-Source Mesh Processing Tool, pp. 129–136. Eurographics Italian Chapter Conference.
- Corradetti, A., Tavani, S., Russo, M., Arbués, P.C., Granada, P., 2017. Quantitative analysis of folds by means of orthorectified photogrammetric 3D models: a case study from Mt. Catria, Northern Apennines, Italy. *Photogramm. Rec.* 32, 480–496.
- Corradetti, A., Zambrano, M., Tavani, S., Tondi, E., Seers, T.D., 2021. The impact of weathering upon the roughness characteristics of a splay of the active fault system

- responsible for the massive 2016 seismic sequence of the Central Apennines, Italy. *Bulletin* 133, 885–896.
- Dershowitz, W.S., Herda, H.H., 1992. Interpretation of Fracture Spacing and Intensity, the 33th US Symposium on Rock Mechanics (USRMS). American Rock Mechanics Association.
- Dong, L., Fang, Y., Lin, W., Seah, H.S., 2015. Perceptual quality assessment for 3D triangle mesh based on curvature. *IEEE Trans. Multimed.* 17, 2174–2184.
- Fernández, O., 2005. Obtaining a best fitting plane through 3D georeferenced data. *J. Struct. Geol.* 27, 855–858.
- Fowles, J., Burley, S., 1994. Textural and permeability characteristics of faulted, high porosity sandstones. *Mar. Petrol. Geol.* 11, 608–623.
- Girardeau-Montaut, D., 2015. Cloud Compare—3d Point Cloud and Mesh Processing Software. Open Source Project.
- Han, H., seek Hong, H., Cho, S., Jeong, J., 2014. Texture Preserving Noise Reduction for Ultra High ISO Images, pp. 415–419, 2014 IEEE Fourth International Conference on Consumer Electronics Berlin (ICCE-Berlin). IEEE.
- Hatton, C., Main, I., Meredith, P., 1994. Non-universal scaling of fracture length and opening displacement. *Nature* 367, 160.
- Hodgetts, D., 2013. Laser scanning and digital outcrop geology in the petroleum industry: a review. *Mar. Petrol. Geol.* 46, 335–354.
- Hodgetts, D., Seers, T., Head, W., Burnham, B., 2015. High Performance Visualisation of Multiscale Geological Outcrop Data in Single Software Environment. European Association of Geoscientists & Engineers, pp. 1–5, 77th EAGE Conference and Exhibition 2015.
- Horn, B.K., 1987. Closed-form solution of absolute orientation using unit quaternions. *JOSA A* 4, 629–642.
- Jerald, J., 2015. The VR Book: Human-Centered Design for Virtual Reality. Morgan & Claypool.
- Jones, R., McCaffrey, K., Clegg, P., Wilson, R., Holliman, N.S., Holdsworth, R., Imber, J., Waggott, S., 2009. Integration of regional to outcrop digital data: 3D visualisation of multi-scale geological models. *Comput. Geosci.* 35, 4–18.
- Kirsch, M., Lorenz, S., Zimmermann, R., Andreani, L., Tusa, L., Pospiech, S., Jackisch, R., Khodadadzadeh, M., Ghamisi, P., Unger, G., 2019. Hyperspectral outcrop models for palaeoseismic studies. *Photogramm. Rec.* 34, 385–407.
- Kottayil, N.K., Cheng, I., Punithakumar, K., Basu, A., 2018. Adapting Texture Compression to Perceptual Quality Metric for Textured 3D Models. Springer, pp. 397–405. International Conference on Smart Multimedia.
- Kraus, M., Ertl, T., 2002. Adaptive Texture Maps, pp. 7–15. Proceedings of the ACM SIGGRAPH/EUROGRAPHICS conference on Graphics hardware.
- Kruskal, W.H., Wallis, W.A., 1952. Use of ranks in one-criterion variance analysis. *J. Am. Stat. Assoc.* 47, 583–621.
- La Pointe, P., 2002. Derivation of parent fracture population statistics from trace length measurements of fractal fracture populations. *Int. J. Rock Mech. Min. Sci.* 39, 381–388.
- Labourdette, R., Jones, R.R., 2007. Characterization of fluvial architectural elements using a three-dimensional outcrop data set: Escanilla braided system, South-Central Pyrenees, Spain. *Geosphere* 3, 422–434.
- Le Mouélic, S., L'Haridon, J., Civet, F., Mangold, N., Triantafyllou, A., Massé, M., Le Menn, E., Beaunay, S., 2018. Using Virtual Reality to Investigate Geological Outcrops on Planetary Surfaces, p. 13366. EGU General Assembly Conference Abstracts.
- Lister, D.L., 2004. Modelling fault geometry and displacement for very large networks. Geological Society, London, *Memoirs* 29, 339–355.
- Long, J., Jones, R., Daniels, S., Gilment, S., Oxlade, D., Wilkinson, M., 2019. PS Reducing Uncertainty in Fracture Modelling: Assessing User Bias in Interpretations from Satellite Imagery. AAPG Annual Convention and Exhibition.
- Lyu, W., Ding, P., Zhang, Y., Chen, A., Wu, M., Yin, S., Yu, J., 2019. Refocusable gigapixel Panoramas for immersive VR experiences. *IEEE Trans. Visual. Comput. Graph.* 27 (3), 2028–2040.
- Masoud, A., Koike, K., 2006. Tectonic architecture through Landsat-7 ETM+/SRTM DEM-derived lineaments and relationship to the hydrogeologic setting in Siwa region, NW Egypt. *J. Afr. Earth Sci.* 45, 467–477.
- McCormack, D.C., Irving, D.H., Brocklehurst, S.H., Rarity, F., 2008. Glacial geomorphological mapping of Coire Mhic Fhearchair, NW Scotland: the contribution of a high-resolution ground based LiDAR survey. *J. Maps* 4, 315–331.
- Mountney, N.P., Thompson, D.B., 2002. Stratigraphic evolution and preservation of aeolian dune and damp interdune strata: an example from the Triassic Helsby Sandstone Formation, Cheshire Basin, UK. *Sedimentology* 49, 805–833.
- Munafò, J., Diedrick, M., Stoffregen, T.A., 2017. The virtual reality head-mounted display Oculus Rift induces motion sickness and is sexist in its effects. *Exp. Brain Res.* 235, 889–901.
- Pearce, M.A., Jones, R.R., Smith, S.A., McCaffrey, K.J., 2011. Quantification of fold curvature and fracturing using terrestrial laser scanning. *AAPG Bull.* 95, 771–794.
- Priddy, C.L., Pringle, J.K., Clarke, S.M., Pettigrew, R.P., 2019. Application of photogrammetry to generate quantitative geobody data in ephemeral fluvial systems. *Photogramm. Rec.* 34, 428–444.
- Priest, S., Hudson, J., 1981. Estimation of Discontinuity Spacing and Trace Length Using Scanline Surveys. In: *International Journal of Rock Mechanics and Mining Sciences & Geomechanics Abstracts*. Elsevier, pp. 183–197.
- Priest, S.D., 2012. *Discontinuity Analysis for Rock Engineering*. Springer Science & Business Media.
- Pringle, J., Howell, J., Hodgetts, D., Westerman, A., Hodgson, D., 2006. Virtual outcrop models of petroleum reservoir analogues: a review of the current state-of-the-art. *First Break* 24, 33–42.
- Rushmeier, H.E., Rogowitz, B.E., Piatko, C., 2000. Perceptual Issues in Substituting Texture for Geometry, Human Vision and Electronic Imaging V. International Society for Optics and Photonics, pp. 372–383.
- Seers, T.D., Hodgetts, D., 2016a. Extraction of three-dimensional fracture trace maps from calibrated image sequences. *Geosphere* 12, 1323–1340.
- Seers, T.D., Hodgetts, D., 2016b. Probabilistic constraints on structural lineament best fit plane precision obtained through numerical analysis. *J. Struct. Geol.* 82, 37–47.
- Stefano, T., Tavan, P., Arbués, Marco, Snidero, Núria, Carrera, 2011. Open Plot Project: an open-source toolkit for 3-D structural data analysis. *Solid Earth* 2 (1), 53–63.
- Stevens, J., Kincaid, J.P., 2015. The effect of visual display on performance in mixed reality simulation. *Int. J. Model. Simulat.* 35, 20–26.
- Sturzenegger, M., Stead, D., 2009. Close-range terrestrial digital photogrammetry and terrestrial laser scanning for discontinuity characterization on rock cuts. *Eng. Geol.* 106, 163–182.
- Sturzenegger, M., Yan, M., Stead, D., Elmo, D., 2007. Application and limitations of ground-based laser scanning in rock slope characterization. Proceedings of the first Canadian US rock mechanics symposium 29–36.
- Tavani, S., Corradetti, A., Granado, P., Snidero, M., Seers, T.D., Mazzoli, S., 2019. Smartphone: an alternative to ground control points for orienting virtual outcrop models and assessing their quality. *Geosphere* 15, 2043–2052.
- Tavani, S., Granado, P., Riccardi, U., Seers, T., Corradetti, A., 2020a. Terrestrial SfM-MVS photogrammetry from smartphone sensors. *Geomorphology* 367, 107318.
- Tavani, S., Pignatola, A., Corradetti, A., Mercuri, M., Smeraglia, L., Riccardi, U., Seers, T., Pavlis, T., Billi, A., 2020b. Photogrammetric 3D model via smartphone GNSS sensor: workflow, error estimate, and best practices. *Rem. Sens.* 12, 3616.
- Thiele, S.T., Grose, L., Samsu, A., Micklethwaite, S., Vollgger, S.A., Cruden, A.R., 2017. Rapid, semi-automatic fracture and contact mapping for point clouds, images and geophysical data. *Solid Earth* 8, 1241.
- Tyrell, R., Sarig-Bahat, H., Williams, K., Williams, G., Treleaven, J., 2018. Simulator sickness in patients with neck pain and vestibular pathology during virtual reality tasks. *Virtual Real.* 22, 211–219.
- Umili, G., Ferrero, A., Einstein, H., 2013. A new method for automatic discontinuity traces sampling on rock mass 3D model. *Comput. Geosci.* 51, 182–192.
- Vasuki, Y., Holden, E.-J., Kovesi, P., Micklethwaite, S., 2014. Semi-automatic mapping of geological Structures using UAV-based photogrammetric data: an image analysis approach. *Comput. Geosci.* 69, 22–32.
- Vollgger, S.A., Cruden, A.R., 2016. Mapping folds and fractures in basement and cover rocks using UAV photogrammetry, Cape Liptrap and Cape Paterson, Victoria, Australia. *J. Struct. Geol.* 85, 168–187.
- Voorn, M., Exner, U., Barnhoorn, A., Baud, P., Reuschlé, T., 2015. Porosity, permeability and 3D fracture network characterisation of dolomite reservoir rock samples. *J. Petrol. Sci. Eng.* 127, 270–285.
- Wakeford, Z.E., Chmielewska, M., Hole, M.J., Howell, J.A., Jerram, D.A., 2019. Combining thermal imaging with photogrammetry of an active volcano using UAV: an example from Stromboli, Italy. *Photogramm. Rec.* 34, 445–466.
- Wang, K., Torkhani, F., Montanvert, A., 2012. A fast roughness-based approach to the assessment of 3D mesh visual quality. *Comput. Graph.* 36, 808–818.
- Woodcock, N., 1977. Specification of fabric shapes using an eigenvalue method. *Geol. Soc. Am. Bull.* 88, 1231–1236.
- Zhang, H., 2017. Head-mounted display-based intuitive virtual reality training system for the mining industry. *Int. J. Min. Sci. Technol.* 27, 717–722.